

Status of the LHCb experiment

CERN-RRB-2018-099

31 October 2018

1 Introduction

The 2018 run is proceeding very smoothly for LHCb. No major modifications were applied for the data taking operations with respect to 2017, with the aim of having highly stable running conditions. The experiment has currently collected about 2.0 fb^{-1} this year and aims to collect close to 2.5 fb^{-1} by the end of 2018 operations. This is the final year of running for the current LHCb experiment which will in total have collected over 9 fb^{-1} .

The operational efficiency is 90% and all subdetectors are running in a very stable way. A flexible trigger strategy is in place that allows LHCb to take data in diverse beam conditions, profiting from all useful luminosity to perform physics studies. More information can be found in Secs. 2 and 3.

The year 2018 has been highly successful for the LHCb physics output, with 31 papers already submitted to journals, in line with the previous years. In total 447 papers have now been published or submitted. Very recently LHCb has announced results on three new particles: evidence has been obtained for an exotic hadron that was named the $Z_c^-(4100)$; the discovery of the $\Sigma_b(6097)^+$ and $\Sigma_b(6097)^-$ was also reported. Highlights since the last RRB include the measurement of the CKM angle γ using $B^\pm \rightarrow DK^\pm$ with $D \rightarrow K_S^0 \pi^+ \pi^-$, $K_S^0 K^+ K^-$ decays, the most precise single measurement determination of γ [1], and the update of the LHCb combination of γ , providing the more precise measurement to date [2]; the measurement of CP asymmetries in two-body $B_{(s)}^0$ -meson decays to charged pions and kaons, providing the first strong evidence of CP violation in $B_s^0 \rightarrow K^+ K^-$ decays [3]; the first observation of the doubly charmed baryon decay $\Xi_{cc}^{++} \rightarrow \Xi_c^+ \pi^+$ [4] and the first measurement of the Ξ_{cc}^{++} lifetime [5]; a new measurement of the Ω_c^0 baryon lifetime [6], which turned out to be four times larger than the current world average; and the first measurement of antiproton production in pHe collisions at $\sqrt{s_{NN}} = 110 \text{ GeV}$ [7], a striking result from LHCb's unique fixed target physics programme. These and other results are discussed in Sect. 4.

Much of our efforts are invested into preparations for the LHCb Upgrade I, which will be installed in Long Shutdown 2. This work is described in a separate

document [8].

2 Detector sub-systems

The LHCb experiment is operating very smoothly in the final year of Run 2 and only minor issues were reported. The magnet tripped a few times due to electrical glitches and a failure of the power converter. Some maintenance work has been performed on the large overhead crane during Technical Stop 2 and renovation of the diesel network has started. Further maintenance work for the cooling and ventilation was performed. Leaks on one of the cooling systems have been observed, but the loss of fluids is marginal and will not affect the data taking. Preparations for the dismantling of some detectors, prior to insertion of the LHCb Upgrade I, are highly advanced. The Long Shutdown 2 will start on the 3rd December, starting with the removal of part of the shielding between UXA and UXB.

2.1 Vertex Locator (VELO)

The VELO continues to perform very efficiently, in spite of the extremely high integrated radiation to which it has now been subjected. The running is efficiently covered by a dedicated team of piquets and on-call experts who continuously monitor the health of the detector and coordinate with external groups such as the TE-VSC for vacuum related issues. The radiation damage is regularly monitored with frequent IV scans which check the patterns of current consumption and the temperature stability and when possible CCE (charge collection efficiency) scans which directly track the effective depletion voltages, Fig. 1. The behaviour is in line with the expectations from radiation models, and as expected it has been necessary to raise the voltages again this year, with the majority of the VELO now operating at 350V. This is an operational challenge as trips in the system are to be avoided to maintain maximum operational efficiency. The voltage supply trip monitoring and triggering system has been modified to avoid spurious trips based on instantaneous fluctuations and the monitoring software has been reinforced to track the changes efficiently. Many sensors have now developed post irradiation currents which have significant voltage dependence. Due to this, many sensors are expected to reach levels approaching 0.5 mA by the end of the year. This is still well within the capability of the HV system, however careful monitoring is necessary due to the sensitivity to temperature fluctuations.

Due to the current consumption, the performance of the cooling system remains key to stable VELO operation. There has been a gradual increase in temperatures, in particular on one side of the VELO, which has been triggered by a number of causes related to the extended age of the system, but is likely dominated by the performance of the insulation of the long transfer lines between the cooling plant and the VELO gradually deteriorating over time. The VELO temperature is kept as low as possible by a number of protective measures. The front end ASIC operat-

ing parameters have been carefully reviewed based on the experience accumulated to date and with lab measurements. Based on this a new set of parameters have been found which lead to improvements in both power consumption and spill over performance and these new parameters have been implemented, resulting in a saving of more than one degree across the VELO. During the recent technical stop a cooling filter has been replaced, improving the performance by roughly one degree. The cooling continues to be monitored and watched carefully.

After eight years of VELO operation, during which cooling interventions and incidents have been minimal and hence the detector has been kept well below zero, the VELO is still in the nominal beneficial annealing regime with respect to depletion voltage behaviour. Due to this, it was decided to deliberately warm the detector to room temperature for two days during the recent technical stop. This is expected to give a further benefit to the most irradiated regions of the detector, reducing the depletion voltage by about 50V. This is expected to considerably ease the operational challenges and should result in an improved VELO performance and eliminate the need to raise the voltages again before the end of the run.

Operationally the major remaining concern has been the performance of the LV supplies, which have needed frequent service and replacement. Recently a modernised DC-DC converter has become available and is now being systematically replaced in the serviced modules.

Detailed plans are being put in place for the VELO dismantling and removal at the end of the year. The detector itself and the majority of the cables and electronics in proximity will be disposed of as radioactive waste. The deinstallation procedure of the VELO detectors and RF foils is complex and will essentially reverse the installation steps. The parts which remain in the vacuum tank, in particular the bellow system, will be surveyed and verified for upgrade operation. The cooling platform must be modified to accommodate the arrival of the new cooling system, and this will be done in a two-step process; allowing for the essential vacuum and motion control system signal cables to be reinstalled and verified in advance of the new hardware installation.

2.2 Silicon Tracker (ST)

The Silicon Tracker (ST), which comprises the Tracker Turicensis (TT) and Inner Tracker (IT), is performing well in its final months of operation. The fraction of working channels in the TT and IT is currently 98.92% and 98.86%, respectively.

The fraction of working channels in the TT is about 0.35% lower than the value reported in the previous RRB document due to desynchronisation errors in the readout electronics of one module. The cause of this desynchronisation is still under investigation. One TT HV channel (corresponding to a sensor in TTaU-RegionBSector4) has been drawing no current since August 2017, and remains disabled for 2018 data-taking. One VCSEL diode in the IT was found to have broken towards the end of YETS. Since a replacement of this diode would have required the opening of the IT half-stations, and only 0.1% of the total sub-detector

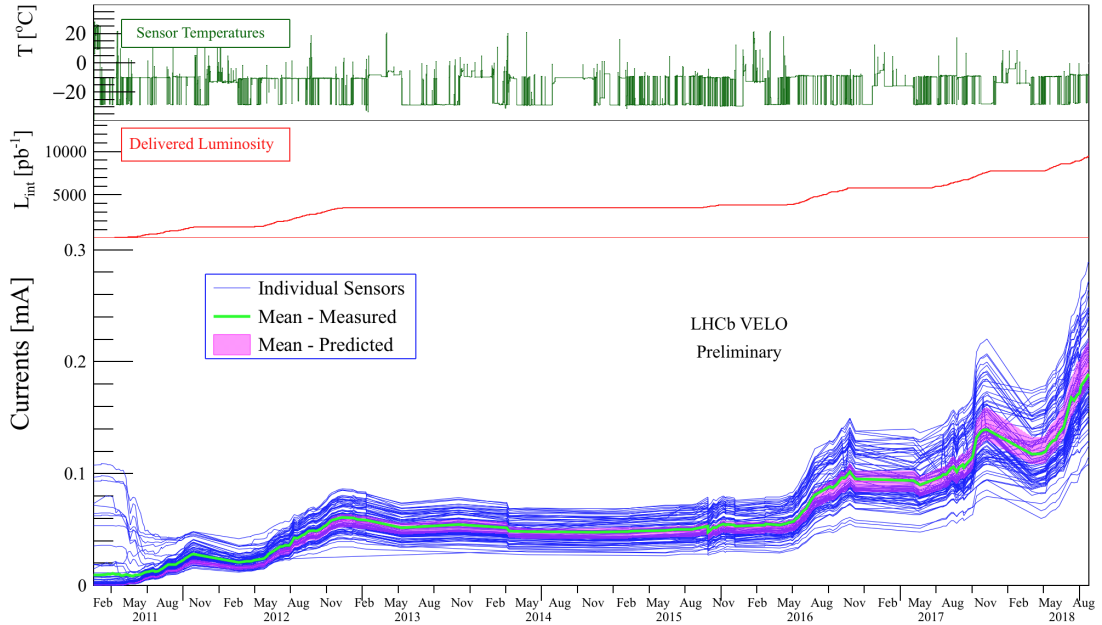


Figure 1: Evolution of VELO currents since 2011. The operational temperatures and delivered luminosity are included.

readout in a low occupancy region was affected, this link remains disabled for 2018. No impact on data quality has been observed due to the loss of these channels.

There have been a few other minor problems in 2018. One TT CAEN High Voltage (HV) board with a faulty channel has been replaced. During replacement of the board, the key of the Primary Power Supply (PPS) unit of the HV CAEN crate failed; the faulty PPS unit has been replaced. A broken VCSEL diode in the TT was replaced just before the start of data-taking in 2018.

An increase in the coolant loss rate of the IT C_6F_{14} cooling circuit has been observed since early June. A preliminary check of the IT manifolds found only a leak near a valve of the C-side manifold, previously observed in 2017 and reported in the previous RRB document. A more extensive leak search will be performed at the next Technical Stop.

Radiation damage in the sensors is monitored via continuous measurements of the leakage current, and depletion voltage measurements obtained from Charge Collection Efficiency (CCE) scans taken periodically during the year. Trends in data collected in 2018 are consistent with predictions from simulation. A paper summarising radiation damage monitoring for the TT from 2011-2017 has been submitted for publication [9].

A Brandeis CCD Angle Monitor (BCAM) based system was installed during LS1 to monitor the movement of the IT half-stations. The system consists of eight BCAM sensors (four for IT1, two each for IT2 and IT3) that observe retro-reflective targets placed on each half-station, and performs a measurement approximately

every 18 seconds. The overall scale of movement of the stations in 2018 is consistent with that seen in previous years. An internal note summarising measurements from 2015-2017 has been prepared.

2.3 Outer Tracker (OT)

The Outer Tracker detector (OT) is in good shape. The year 2018 is the last year of operation of the OT, after about 10 years of successful data taking. The OT did not suffer from significant operational problems during its entire lifetime, and data taking in 2018 went particularly smooth. No sign of performance degradation has been observed, due to radiation damage or simple ageing or otherwise. In addition, no intervention during 2018 was necessary that required the opening of the tracking stations, and thus the stability of the alignment was guaranteed. The number of noisy channels was negligible ($<0.1\%$ of the straws with $\sim 1\%$ of noise hits), as was the error rate from sporadic desynchronizations of single chips here and there. (To reduce the noise for 16 straws, the amplifier threshold was increased slightly, whereas the error rate was reduced by replacing a single front-end during the EYETS before 2018.) The number of unresponsive straws was below 0.1% , of which the largest part came from a short circuit in the HV system affecting 32 straws on the outside of station T1. During the 2018 run LHCb received the maximal number of 2332 colliding bunches. The large instantaneous luminosity of $4.6 \cdot 10^{32} \text{ cm}^{-2} \text{ s}^{-1}$ was about twice the instantaneous design luminosity, but the currents in the OT were about 30% lower than the trip level. The data rate from the OT reaches its limit above 1 MHz readout rate, this was taken into account in the optimization of the thresholds of the lowest trigger level (L0). The rejection of 7% of events where the previous event was busy limited the bandwidth needed for useless spill-over hits. The real-time calibration of the global timing offset guaranteed an excellent timing measurement. A resolution for a time-stamp of 0.6 ns is achieved, and its use for physics analyses is being studied. A document summarizing the Outer Tracker performance in Run2 can be found at JINST 12 (2017) P11016 [arXiv:1708.00819 [hep-ex]].

A detailed plan has been prepared for the dismantling procedure of the OT detector after the end of data taking. The 12 C-frames - with all detector modules and front-end units mounted - will be placed in a single steel frame. The frame will be transported to the surface, and then transported to the storage building on the Preveessin site for radiation cooldown. At the end of the long shutdown 2, the modules and electronics will be unmounted. Special care in the dismantling will be taken, to allow the re-use of (part of) the detector by other interested parties.

2.4 RICH system

The RICH detectors have been working extremely well in 2018 with no software or hardware issues to report. All the required maintenance took place during the YETS at the end of 2017. Two HPDs at the edge of RICH 2 stopped working

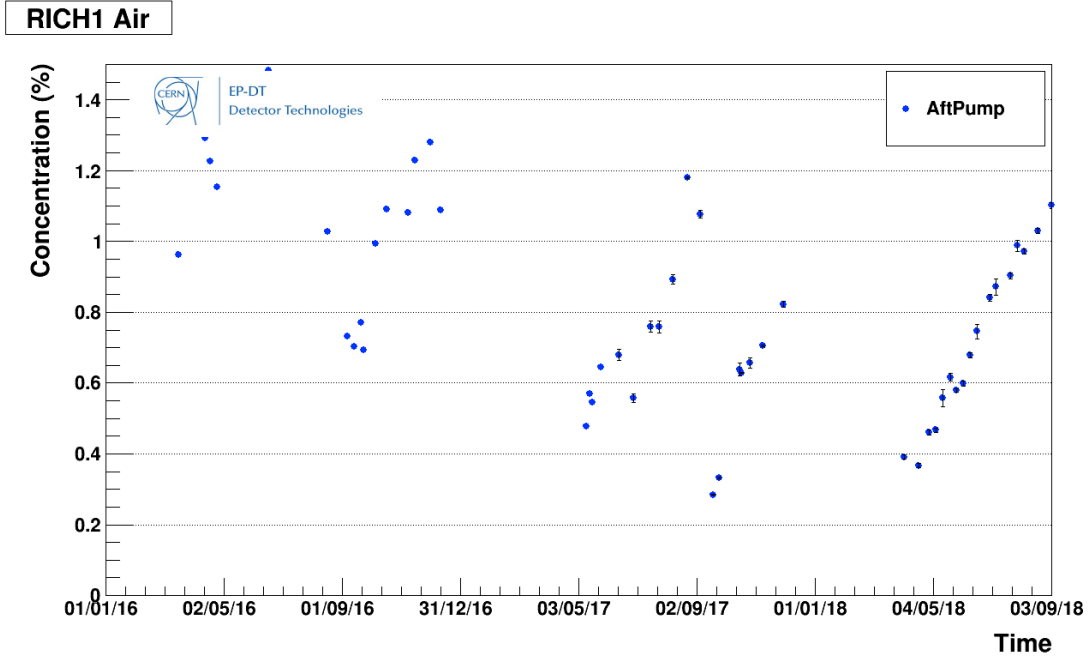


Figure 2: Air contamination in RICH 1 since January 2016. The gas is cleaned when the concentration reaches approximately 1%.

early into the run of 2018, but it was decided not to intervene as they are at the edge of the acceptance. No further maintenance is expected before the end of the year and the dismantling of the current detectors. The air contamination of the C_4F_{10} gas in RICH 1 has been followed closely over the years and a procedure for cleaning the gas during a Technical Stop (TS) without first emptying the whole volume was introduced during LS1. Since 2015, pure C_4F_{10} is introduced in RICH 1 at the start of the year and it is cleaned again once during the year when the contamination has reached approximately 1%. Fig. 2 shows the amount of air in RICH 1 since January 2016. The RICH 1 gas will be cleaned again during the September TS. A full Upgrade detector module was installed in RICH 2 and is operating in parallel with the LHCb acquisition system using the LHCb trigger decisions. It has been possible to detect light synchronous with the LHC collisions and get valuable experience with the Upgrade DAQ system and operation of the Upgrade front-end electronics.

2.5 Calorimeters (SPD, PS, ECAL and HCAL)

The Calorimeter system is running smoothly during the 2018 LHC run. So far, all cells in SPD and PS are working fine; there are only two dead cells in ECAL and three in HCAL detected. Out of the other problems in the Calorimeter system operation, the one to be mentioned here is the instability in the timing in one of

the ECAL crates (#19), which occurs from time to time since the end of August. The effect on the data quality is negligible, however, the controller of this crate was replaced during Technical Stop 2. The procedure of calibration of the Calorimeters in 2018 is quite similar to that during the 2017 data taking and has been shown to work nicely and to be effective:

- The HCAL calibration with ^{137}Cs source was performed before the run, on March 23, 2018, and then subsequently at every technical stop;
- The time alignment constants of all the Calorimeters were updated using the data from first collisions in April 2018;
- The ECAL absolute calibration based on $\pi^0 \rightarrow \gamma\gamma$ is now setup in a fully automatic mode: it is launched on achieving the required number of calibration events. It is performed roughly once per month, as of April 24th 2018;
- The LED monitoring systems of ECAL and HCAL are used for PMT HV correction after each fill. This procedure is running since 2015 and it stabilizes the PMT gains during the periods between absolute calibrations of ECAL and HCAL.

Summarizing, the calorimeter detectors in 2018 are taking data efficiently and without significant hardware problems.

2.6 Muon system

During 2018 data taking, the muon chambers have been operating in a very stable manner for many months, with station efficiencies exceeding 99%. This is illustrated in Fig. 4, where the track illumination on the five stations is shown for a fill at the end of the summer. Only a couple of local inefficiency spots are present in the whole detector, with negligible impact on the overall detector performance. During 2018, the number of gaps suffering from HV trips in the presence of beam were 56. This is the same level as measured during 2017 and a factor of two less than in 2016, which denotes a positive trend in the operation of the detector. All of the above represents a remarkable success for a system made of 1380 chambers (with four gaps each) and 122112 front-end channels, and after almost ten years of operation. More importantly, the fact that no ageing effects are visible so far is very reassuring, as the same chambers will be operated up to the end of Run 4 (except for M1 station, which will be dismantled during LS2). To achieve this smooth operation, the gaps affected by high currents are successfully trained during data taking, with positive HV polarity, and during the YETS, with negative HV polarity.

Another crucial ingredient to ensure a successful operation during the forthcoming years is careful preparatory work of equipping an adequate stock of spare

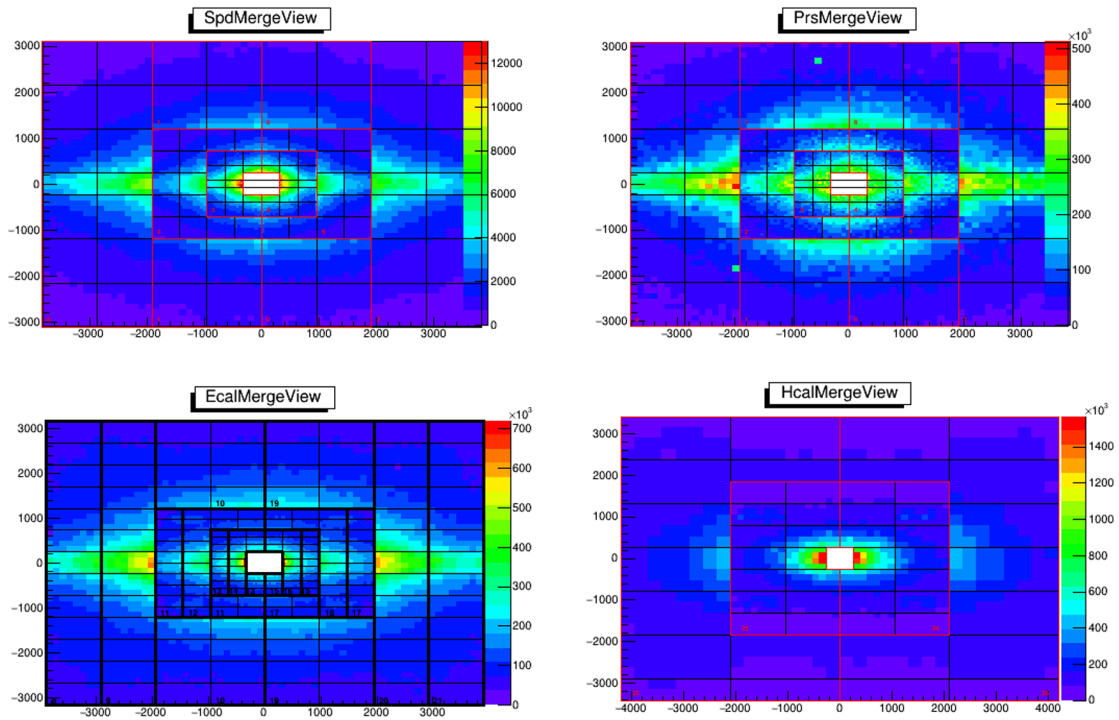


Figure 3: Average transverse energy in a cell of CALO detectors in arbitrary units, 200k events,

chambers. This task is accomplished in the muon experimental area at building 169, where the recently produced spare MPWCs are being dressed with FE-electronic boards. Those chambers are tested together with others from previous productions, for a total number of spare MWPC chambers of about 150 for stations M2 to M5, or $\sim 15\%$ of the installed chambers. In the same area, a special buffer zone is being prepared for temporary storage of the 252 MWPCs belonging to the M1 station, which will be dismantled in spring next year. These chambers will be used as additional spare material, particularly for the front-end electronics.

2.7 Forward shower counters (HeRSChel)

The HERSCHEL sub-detector has been employed in LHCb data-taking throughout 2018, and operation of the re-commissioned detector, after the 2017-2018 replacement campaign, has been smooth. Work continued on the integration of the HERSCHEL front-end board in the standard LHCb hardware trigger, with major progress being made to overcome faulty hardware (one of two available L0 selection boards malfunctioned) and timing challenges (the standard $4\mu s$ window is too narrow to incorporate information from the furthest B2 and F2 stations), as well

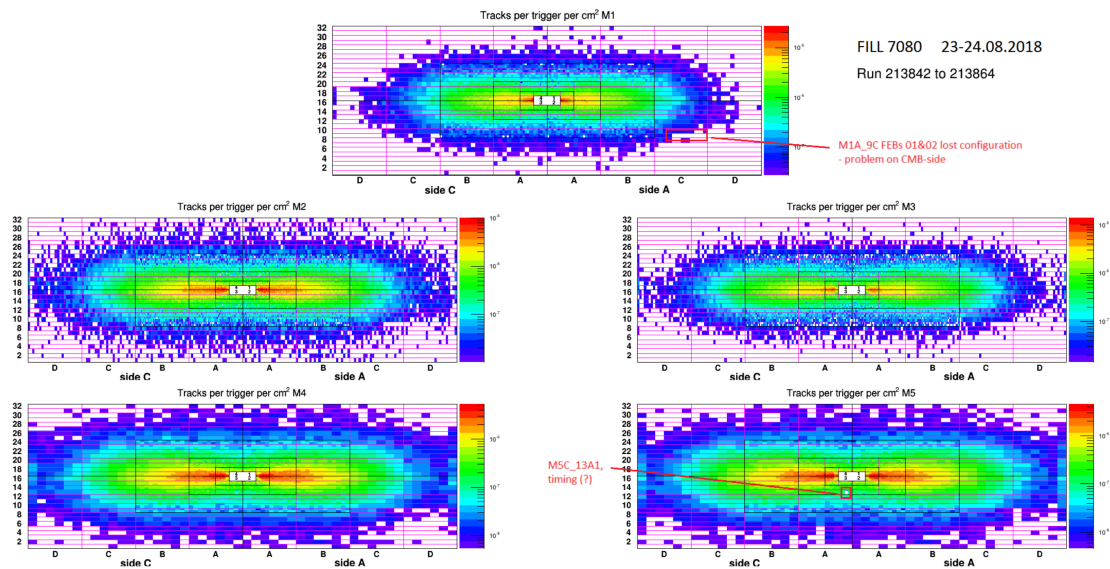


Figure 4: Track density as measured in normal data taking at the end of August 2018 on the five stations of the muon detector.

as a re-write of the front-end trigger FPGA firmware. Daily, automated, updates to the HV settings and time-alignment of the detector were implemented in order to combat the effects of radiation damage on the counters, allowing HERSCHEL to provide a stable input to the trigger. HERSCHEL information has been in use in the L0 for CEP lines since early July, with over 1.5 fb^{-1} expected to be collected where HERSCHEL has played a role in the hardware trigger.

Offline, following the publication of the HERSCHEL performance paper in JINST [13 (2018) P04017], analyst use of HERSCHEL information has continued to grow. A centrally-available HERSCHEL-activity metric has been deployed for 2015 and 2016 data, and is expected soon for 2017, and the first analysis to use HERSCHEL is in the final stages of JHEP journal review.

Plans are converging for the dismantling of the HERSCHEL counters and the removal of the supporting frames from the LHC tunnel after 2018 data-taking is completed, on a timescale designed to provide the necessary access to the occupied space for the various LHC groups requiring it.

2.8 Online system

The Online system ran very stably during the 2018 data taking. The inefficiency due to the Data Acquisition System (DAQ) so far was $\sim 2\%$, where 80% of this is attributable to problems in the sub-detector DAQ.

The HLT farm is used up to its maximum capacity with the High-Level Trigger processes and, whenever possible, with Monte-Carlo production, as shown in Fig. 5. The usage of the disk buffer between HLT1 and HLT2 reached its maximum

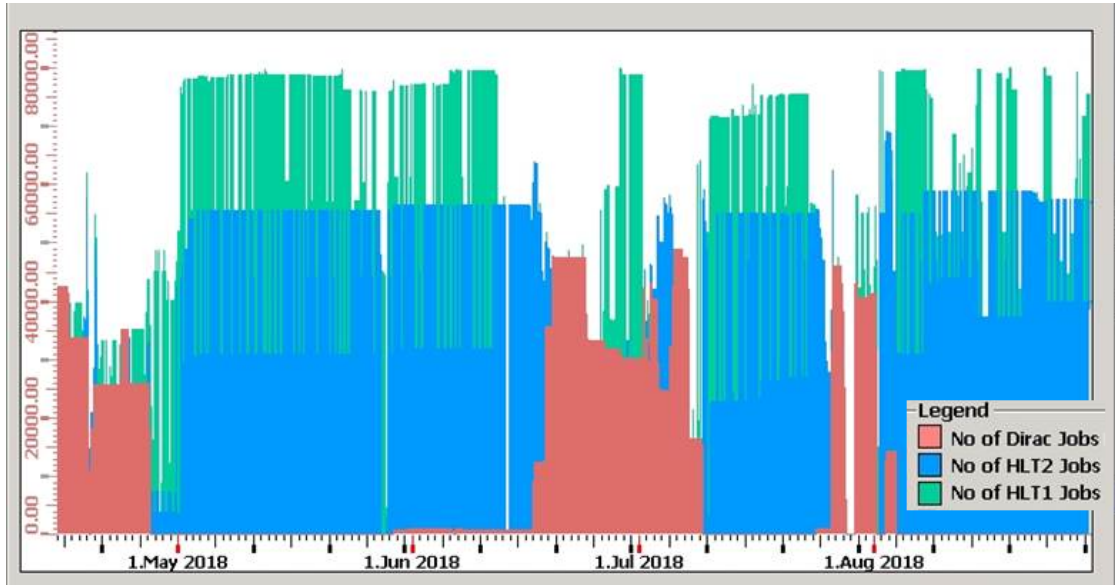


Figure 5: Number of processes running on the HLT farm.

($\sim 40\%$) before the start of Machine Development period MD3. The buffer will be emptied before the restart after Technical Stop (TS) 2. There is no appreciable risk that the buffer will significantly fill up before the next MD period (MD4).

Occasionally we suffer from broken disks in the farm and old farm nodes failing irreparably. The rate of these incidents is not alarming. For the rest of the year, no changes are foreseen.

The HLT farm will be dedicated fully to Monte-Carlo production throughout TS2, with interruptions only during power and cooling maintenance. At the end of 2019 the farm nodes will be moved from the pit to the newly installed Data Centre at point 8 and MC production will continue.

3 Operations

In 2018 LHCb has recorded at the time of writing a total integrated luminosity of 1.8 fb^{-1} of proton-proton collisions at a centre-of-mass energy of 13 TeV with a global efficiency close to 90%. This is now higher than the luminosity collected in 2017. The $\sim 10\%$ inefficiency is dominated by the irreducible contribution from the electronic deadtime ($\sim 7\%$). Since 2011, LHCb has collected 8.7 fb^{-1} of integrated luminosity with proton-proton collisions, out of 9.5 fb^{-1} delivered by LHC. Fig. 6 summarises the delivered and recorded luminosity in 2018 and for the period between 2011 and 2018.

The last month of the 2018 LHC operations will be dedicated to Pb-Pb collisions. LHCb will collect these data together with data with the SMOG system. The LHCb SMOG system (System for Measuring Overlap with Gas) allows the

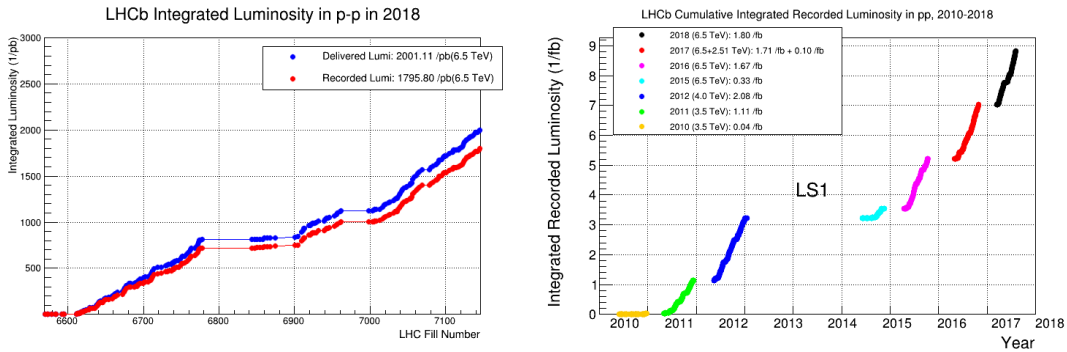


Figure 6: Delivered and recorded integrated luminosity for the 2018 proton-proton run (left) and for the full LHC data taking period since 2011 (right).

injection of small amounts of gas into the beam vacuum in the VELO detector region. This then acts as a fixed target for the LHC beam. The LHCb Data Acquisition is able to collect both collision and fixed-target events in parallel.

3.1 Trigger

In LHCb, the hardware trigger (L0) is followed by a two-stage software trigger. In the Run 2 data taking strategy, after the first trigger stage (HLT1) the data are stored on a disk buffer of the online-farm with a capacity of about 11 PB. The HLT1 processing is performed during the fill, while the second stage of the software trigger (HLT2) is running asynchronously during the fill at a lower rate of about 30 kHz and outside the fill at a rate of about 90 kHz. The deferred HLT2 processing allows the evaluation of the real-time alignment and calibration of the detector, before the data processing. To maximise the selection efficiency within the available computing resources two sets of HLT1 selections were prepared: a tight configuration with an output rate of 95 kHz, and a loose configuration with an output rate of 115 kHz. The loose selection is the default while the tight one is used in the case of a risk to overfill the disk buffer. The risk of overfilling is evaluated by monitoring the disk status and performing a filling projection to the end of the data taking.

During 2018, the beam conditions (number of colliding bunches and the filling scheme) have been uniform throughout the data taking allowing LHCb to take data with the same trigger configuration. In particular, the loose selection has been used for the entire 2018; Fig. 7 shows the disk buffer usage at the end of August and the projection until the end of the year. The risk to exceed the 80% disk usage by the end of the year is 0.3% and thus it is likely that the loose selection will be maintained.

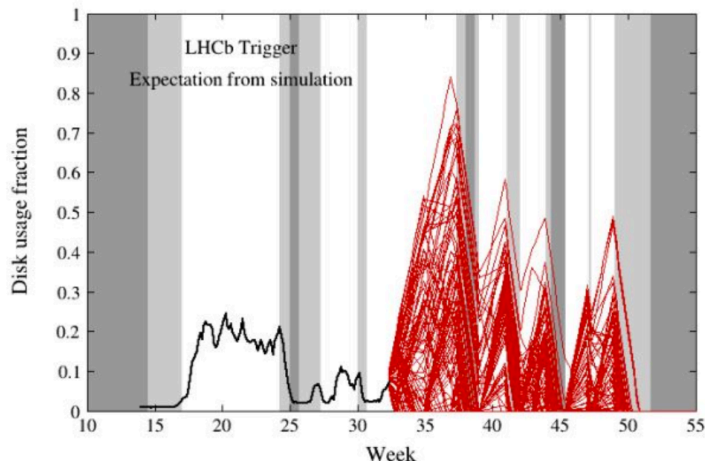


Figure 7: Evolution of the farm disk usage in 2018 (black line) and projection to the end of the 2018 for several toy models based on the assumption of a 50 % LHC availability (red lines).

3.2 Use of the online-farm for Monte Carlo productions

The simulation samples are one of the key elements for the validation of the physics measurements and to evaluate their associated errors. Production of very large simulated data samples is needed to achieve the high precision measurements performed in the ambitious LHCb physics programme. The requests for simulated data production are constantly growing and their processing is using the largest fraction ($\sim 70\%$) of the total computing resources. Efforts are ongoing to provide multiple options for simulating events in a faster way, in particular when high statistics is needed. Two examples are to simulate only partially the detector or to simulate only particles from the signal decay and re-use the underlying event. The fraction of MC productions using one of the faster options steadily increased in the last months and it is now about 20% of the queued requests.

To profit from the available resources and to boost the Monte Carlo production, the online-farm is used for simulation jobs when it is not busy with trigger processing, for example during YETS, technical stops or machine development periods. Fig. 8 shows the jobs running on the online farm during the last months. The technical stops and machine development periods when the farm was fully dedicated to the MC production can be distinguished from the data taking during the pp collisions when only HLT1 and HL2 jobs were running.

3.3 Turbo and Calibration streams

The Turbo stream provides a framework in which physics analysis can be performed directly on the trigger-reconstructed candidates, the only part of the event written on disk. This stream requires a much smaller event size than in the standard data. In 2016, the possibility to save the entire trigger-reconstructed event

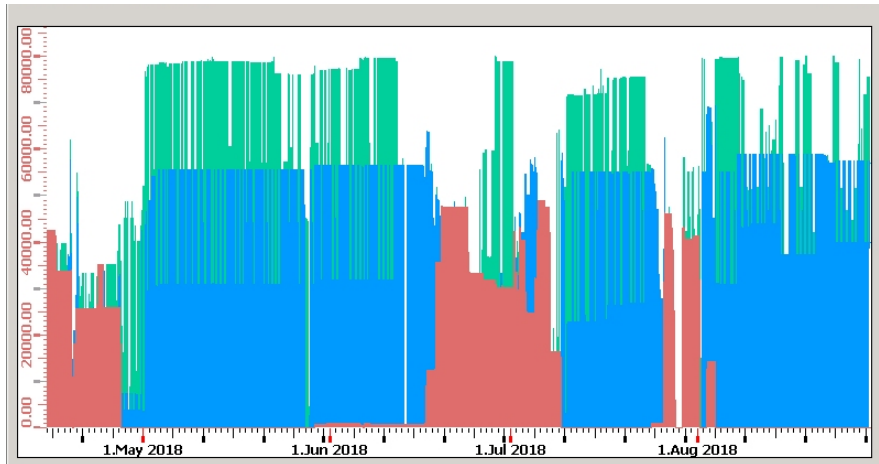


Figure 8: Number of jobs running on the online-farm since the restart of data taking in April 2018: red histograms indicate Monte Carlo jobs, green histograms HLT1 jobs, blue histograms HLT2 jobs.

was also added, and this led to an increase of the Turbo output bandwidth by more than a factor of three and to a significant increase of the Turbo dataset size. To reduce the resources required for this stream without limiting the physics output, the selection of all the lines was optimised and two new features were introduced: each physics analysis in the Turbo stream can be configured to selectively store raw banks or physics objects in addition to those related to the selected decay tree. This was implemented for the 2017 data taking and used for charm spectroscopy where the event size is now reduced by a factor of two without affecting the physics performance. In 2018, more physics analyses use the Turbo stream with a dedicated selection configuration.

The Calibration stream is used to measure efficiencies and other performance parameters directly from the data. Events in the Calibration stream contain the persisted trigger candidates in addition to the raw sub-detector data. This stream is used for the evaluation of the tracking efficiency and for the charged particle identification calibration.

3.4 Real-time alignment and calibration

The real-time alignment and calibration was implemented at the beginning of Run 2 and improved in the following years. This procedure allows to profit from the fully aligned and calibrated detector already in the software trigger. Thanks to this and together with the possibility to run the full reconstruction, the second stage of the software trigger can profit from the best performance both for the tracking and particle identification to maximise the selection efficiency.

The real-time alignment is evaluated on a fill-by-fill basis and is updated when a significant variation is observed. This includes the alignment of the vertex detector,

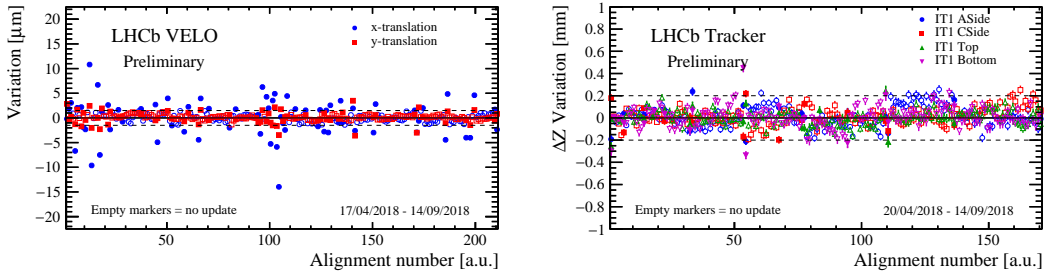


Figure 9: Variation of the VELO (left) and of the IT boxes (right) alignment constants in the first months of 2018 data taking. The dashed lines indicate the minimum variation at which an alignment difference is considered significant. Each point shows the variation of the alignment parameter with respect to the constants used. The full markers indicate when an alignment update was needed.

the tracker system, the muon chambers and the RICH mirrors. For the latter the alignment is updated also after each change of magnet polarity. The calibration is evaluated and updated on a run-by-run basis for the RICH detector and for the global time calibration of the OT, and on a monthly basis for the electromagnetic calorimeter.

All the tasks of the real-time alignment and calibration operated smoothly in 2018. Fig. 9 shows the relative variation of some of the VELO and IT alignment constants with respect to the previous alignment update. Typically the VELO alignment is updated every three fills on average while the tracker alignment is mainly updated only after each magnet polarity change. Fig. 10 shows the relative variation of some of the mirror alignment constants with respect to the previous alignment during data taking.

The absolute calibration of the electromagnetic calorimeter is based on a π^0 sample studied cell by cell. Until 2015, this calibration was performed only offline. Since 2016, there is a fill-by-fill relative calibration by an automatic LED system that allows to evaluate the HV settings needed to compensate the aging of the detector. Starting from 2017, an online absolute calibration has been implemented, which is fully automatised since the beginning of 2018 data taking. The effect of the electromagnetic calorimeter calibration is evaluated using $B^0 \rightarrow K^{*0}\gamma$ events. The B^0 invariant mass resolution is 101.3 ± 0.1 MeV for the uncalibrated sample and 86.2 ± 0.8 MeV (in 2018) for the calibrated sample. Fig. 11 shows the invariant mass of $B^0 \rightarrow K^{*0}\gamma$ for 2018 calibrated sample.

3.5 Data Quality

Data quality control is a key ingredient for the physics results. Since the beginning of Run 2 a new web-based tool has been deployed. The tool has been used to evaluate the offline data quality and as main tool for experts that needed to do remotely quick checks. During the 2018 data taking, the tool has been finalised

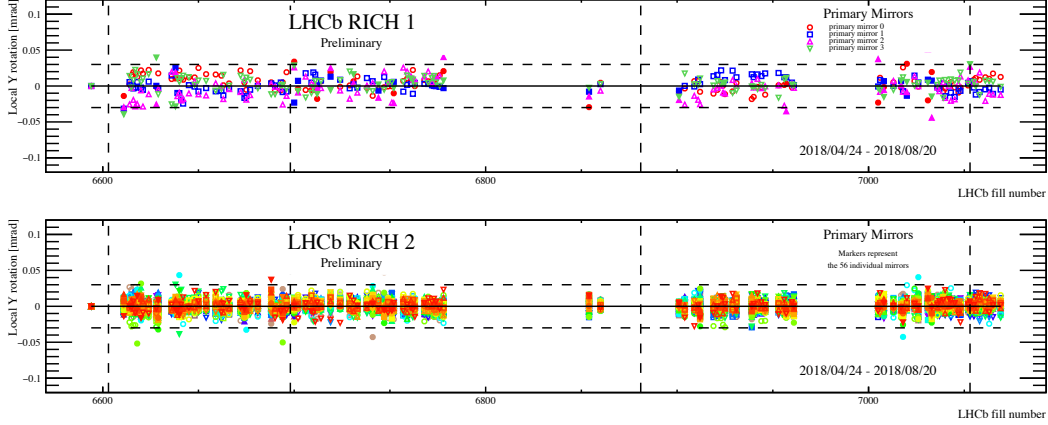


Figure 10: Variation of rotations around the local y-axes of the individual RICH1 (top) and RICH2 (bottom) mirrors for the 2018 data taking. Each point shows the variation of the alignment parameter with respect to the constants in use. The full markers indicate when an alignment update was needed. The horizontal dashed lines indicate the minimum variation to consider significant the alignment difference. The vertical dashed lines indicate changes of magnet polarity.

also for its use during shifts in the control room. The work now focuses on the finalisation of data quality for the simulation productions.

3.6 Computing

The computing usage for 2017 [10], the re-assessed estimates for 2019, incorporating the increased LHC efficiency, and a preview of requests for Run 3 [11], are discussed in detail in separate documents.

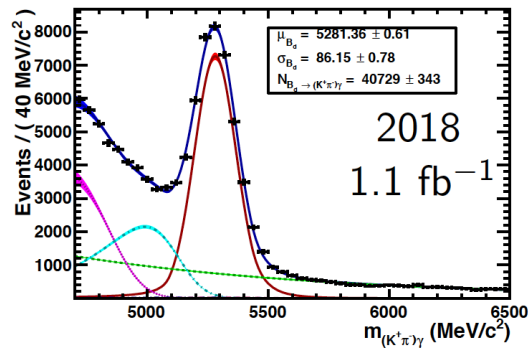


Figure 11: The invariant mass distribution of $B^0 \rightarrow K^{*0} \gamma$ for 2018 data.

4 Physics results

Since the last RRB in April 2018, the LHCb collaboration has submitted 27 new publications, for a total of 447 papers at the time of writing. Ten further publications are being processed by the LHCb Editorial Board and are close to submission. In the following, some selected results from recent publications are highlighted.

4.1 CP violation in beauty and charm

LHCb continues to pursue a wide programme of precision measurements of CP violation in b - and c -hadron decays. In particular, many new measurements were released with sensitivity to the CKM angle γ , with the aim of further improving the precision on the determination of this fundamental parameter of the Standard Model.

The time-dependent CP asymmetries in $B^0 \rightarrow \pi^+\pi^-$ and $B_s^0 \rightarrow K^+K^-$ decays were measured using a data sample of pp collisions corresponding to an integrated luminosity of 3.0 fb^{-1} , collected in LHC Run 1 at centre-of-mass energies of 7 and 8 TeV [3]. The same data sample was used to measure the time-integrated CP asymmetries in $B^0 \rightarrow K^+\pi^-$ and $B_s^0 \rightarrow \pi^+K^-$ decays. The combination of all these measurements can constrain the value of γ [12]. The measured parameters are $C_{\pi^+\pi^-} = -0.34 \pm 0.06 \pm 0.01$, $S_{\pi^+\pi^-} = -0.63 \pm 0.05 \pm 0.01$, $C_{K^+K^-} = 0.20 \pm 0.06 \pm 0.02$, $S_{K^+K^-} = 0.18 \pm 0.06 \pm 0.02$, $A_{K^+K^-}^{\Delta\Gamma} = -0.79 \pm 0.07 \pm 0.10$, $A_{CP}^{B^0} = -0.084 \pm 0.004 \pm 0.003$, and $A_{CP}^{B_s^0} = 0.213 \pm 0.015 \pm 0.007$, where the first uncertainties are statistical and the second systematic. Evidence for CP violation is found in the $B_s^0 \rightarrow K^+K^-$ decay for the first time. The measurements of $C_{\pi^+\pi^-}$, $S_{\pi^+\pi^-}$, $A_{CP}^{B^0}$ and $A_{CP}^{B_s^0}$ are the most precise from a single experiment to date, and are in good agreement with previous determinations

Time-dependent CP asymmetries were also studied in $B^0 \rightarrow D^\mp\pi^\pm$ decays [13]. The coefficients S_f and $S_{\bar{f}}$ are sensitive to $2\beta + \gamma$, although the sensitivity is reduced by a factor $r_{D\pi}$ which is of the order of 0.02. The decays are reconstructed using 3.0 fb^{-1} collected in Run 1. The CP asymmetries were measured to be $S_f = 0.058 \pm 0.020$ (stat) ± 0.011 (syst) and $S_{\bar{f}} = 0.038 \pm 0.020$ (stat) ± 0.007 (syst). These results are used to constrain γ to intervals that are consistent with the current world-average value. In future LHCb upgrades [14], once the γ angle will be known with much higher precision, this analysis can provide a penguin-free measurement of β .

As a further CP violation measurement in B-meson decays, a new measurement of γ was performed using the $B^\pm \rightarrow DK^\pm$ decays, with $D \rightarrow K_S^0\pi^+\pi^-$ and $D \rightarrow K_S^0K^+K^-$ [1]. A binned Dalitz plot analysis has been performed to extract the CP -violating observables x_\pm and y_\pm , which are sensitive to γ using a sample of 2.0 fb^{-1} collected in 2015 and 2016. The values of the CP violation parameters are found to be $x_- = (9.0 \pm 1.7 \pm 0.7 \pm 0.4) \times 10^{-2}$, $y_- = (2.1 \pm 2.2 \pm 0.5 \pm 1.1) \times 10^{-2}$, $x_+ = (-7.7 \pm 1.9 \pm 0.7 \pm 0.4) \times 10^{-2}$, and $y_+ = (-1.0 \pm 1.9 \pm 0.4 \pm 0.9) \times 10^{-2}$, where the first uncertainty is statistical, the second is systematic, and the third

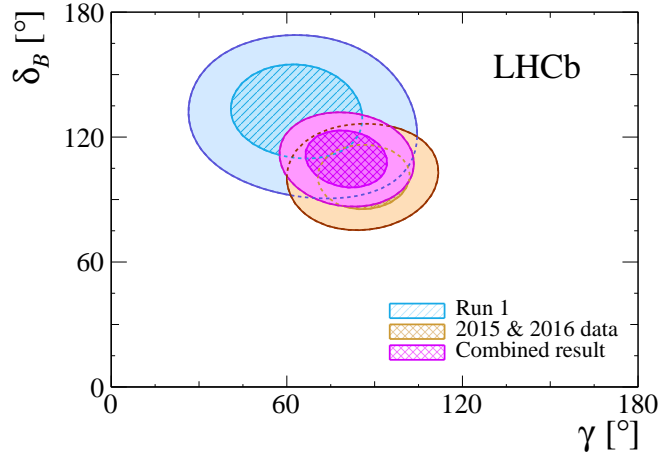


Figure 12: Two-dimensional 68.3% and 95.5% confidence regions for (γ, δ_B) for the x_{\pm}, y_{\pm} parameters obtained in the fit to 2015 and 2016 data, the fit to Run 1 data, and their combination. From an analysis of $B^{\pm} \rightarrow DK^{\pm}$ decays, with $D \rightarrow K_S^0 \pi^+ \pi^-$ and $D \rightarrow K_S^0 K^+ K^-$ [1].

is due to the uncertainty on the strong-phase measurements. These values are used to obtain $\gamma = (87_{-12}^{+11})^{\circ}$, $r_B = 0.087_{-0.014}^{+0.013}$, and $\delta_B = (101 \pm 11)^{\circ}$, where r_B is the ratio between the suppressed and favoured B -decay amplitudes and δ_B is the corresponding strong-interaction phase difference. This measurement is combined with the result obtained using 2011 and 2012 data collected with the LHCb experiment, to give $\gamma = (80_{-9}^{+10})^{\circ}$, $r_B = 0.080 \pm 0.011$, and $\delta_B = (110 \pm 10)^{\circ}$ (Fig. 12). This measurement represents the most precise determination of γ from a single analysis.

A combination of tree-level measurements of the CKM angle γ at LHCb has also been released [2]. The results are obtained from time-integrated measurements of $B^+ \rightarrow DK^+$, $B^+ \rightarrow D^* K^+$, $B^+ \rightarrow DK^{*+}$, $B^0 \rightarrow DK^{*0}$, $B^0 \rightarrow DK^+ \pi^-$ and $B^+ \rightarrow DK^+ \pi^+ \pi^-$ decays and time-dependent analyses of $B_s^0 \rightarrow D_s^{\mp} K^{\pm}$ and $B^0 \rightarrow D^{\mp} \pi^{\pm}$ decays. This combination includes new and updated results compared to the previous LHCb combination, giving a best fit value of $\gamma = 74.0^{\circ}$ with confidence intervals, set using a frequentist procedure, of $\gamma \in [68.2, 79.0]^{\circ}$ at 68.3% confidence level (CL) and $\gamma \in [61.6, 83.7]^{\circ}$ at 95.5% CL, where all values are modulo 180° . This gives the result $\gamma = (74.0_{-5.8}^{+5.0})^{\circ}$, where the uncertainty includes both statistical and systematic contributions. The results are summarised in Fig. 13. The result for γ is consistent with the averages obtained by CKMfitter, UTFit, and HFLAV: $\gamma = (73.2_{-7.0}^{+6.3})^{\circ}$ [15], $\gamma = (68.3 \pm 7.5)^{\circ}$ [16] and $\gamma = (73.5_{-5.1}^{+4.2})^{\circ}$ [17]. It is also consistent with the previous LHCb average, $\gamma = (76.8_{-5.7}^{+5.1})^{\circ}$ [18], and is the most precise determination of γ from a single experiment to date.

LHCb continues the search for CP violation in charmed hadrons, exploiting the largest charm sample ever collected by an experiment. A study of $D^0 \rightarrow \pi^+ \pi^- \mu^+ \mu^-$

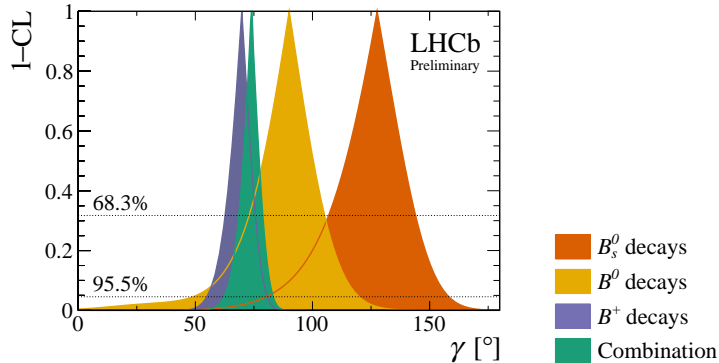


Figure 13: $1 - \text{CL}$ plots, using the profile likelihood method, for combinations split by the initial B meson flavour: (orange) B_s^0 initial states, (yellow) B^0 initial states, (blue) B^+ initial states and (green) the full combination.

and $D^0 \rightarrow K^+ K^- \mu^+ \mu^-$ has been performed [19] in which their branching fractions were measured to be $(9.6 \pm 1.2) \times 10^{-7}$ and $(1.54 \pm 0.33) \times 10^{-7}$, respectively, in agreement with SM predictions. Despite the tiny branching fractions, LHCb collected enough of these decays to perform a study of angular and CP asymmetries in these decays [20]. These asymmetries are predicted to be negligibly small in the SM but could be as large as $\mathcal{O}(1\%)$ in scenarios of physics beyond the SM. The first measurements of the forward-backward asymmetry of the dimuon pair (A_{FB}), the triple-product asymmetry ($A_{2\phi}$), and the charge-parity-conjugation asymmetry (A_{CP}), has been performed using 5 fb^{-1} of data collected from 2011 to 2016. The asymmetries are also measured as a function of the dimuon invariant mass. The results are consistent with the Standard Model predictions.

4.2 Hadron production and decays

LHCb continues to explore hadron production and decay mechanisms through a wide and successful programme including, among other things, a large number of heavy-flavour spectroscopy studies and many precise lifetime measurements.

The doubly charmed baryon Ξ_{cc}^{++} was observed for the first time in 2017 in the decay channel $\Xi_{cc}^{++} \rightarrow \Lambda_c^+ K^- \pi^+ \pi^+$ [4]. A second observation, confirming the discovery, has now been made in the decay channel $\Xi_{cc}^{++} \rightarrow \Xi_c^+ \pi^+$ with a statistical significance of 5.9σ [21]. The data sample used corresponds to an integrated luminosity of 1.7 fb^{-1} collected in Run 2. The measured Ξ_{cc}^{++} mass in this new decay mode is $3620.6 \pm 1.5 \text{ (stat)} \pm 0.4 \text{ (syst)} \pm 0.3 \text{ (}\Xi_c^+\text{)} \text{ MeV}/c^2$, consistent with the previous result.

Using the same data sample, LHCb also reported the first measurement of the Ξ_{cc}^{++} lifetime [5], with the Ξ_{cc}^{++} baryon reconstructed through the decay chain $\Xi_{cc}^{++} \rightarrow \Lambda_c^+ K^- \pi^+ \pi^+$, $\Lambda_c^+ \rightarrow p K^- \pi^+$. The measured lifetime is $0.256^{+0.024}_{-0.022} \text{ (stat)} \pm 0.014 \text{ (syst)} \text{ ps}$, which establishes the weakly decaying nature of the Ξ_{cc}^{++} state.

Using an analysis technique similar to that used for the Ξ_{cc}^{++} lifetime mea-

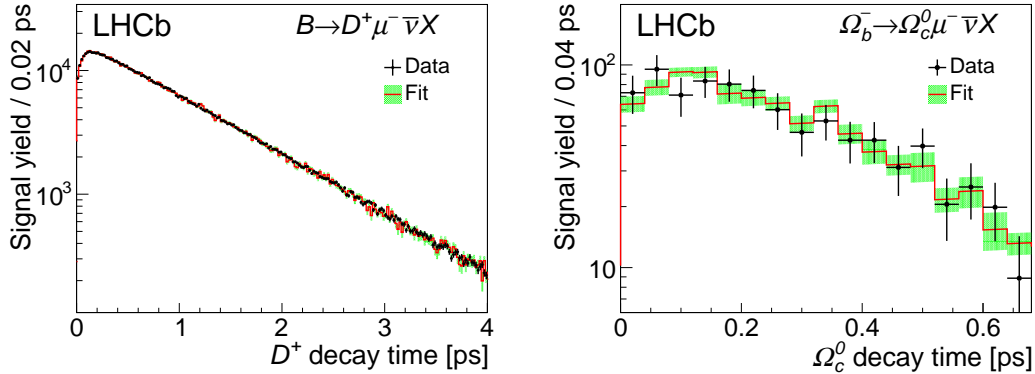


Figure 14: Decay-time spectra for (left) D^+ signal in $B \rightarrow D^+ \mu^- X$ events and (right) Ω_c^0 signal in $\Omega_b^- \rightarrow \Omega_c^0 \mu^- X$ events. Overlaid are the fit results along with the uncertainties due to finite simulated sample sizes.

surement, the lifetime of the Ω_c^0 baryon has been measured using the full Run 1 data sample [6]. About 1000 $\Omega_b^- \rightarrow \Omega_c^0 \mu^- \bar{\nu}_\mu X$ signal decays have been selected, where the Ω_c^0 baryon is detected in the $pK^-K^-\pi^+$ final state and X represents possible additional undetected particles in the semileptonic decay. The Ω_c^0 lifetime is measured relative to that of the D^+ meson (see Fig. 14), and is found to be $\tau_{\Omega_c^0} = 268 \pm 24 \pm 10 \pm 2$ fs, where the uncertainties are statistical, systematic, and from the uncertainty in the D^+ lifetime, respectively. This value is nearly four times larger than, and inconsistent with, the current world-average value of 69 ± 12 fs [22]. With this measurement, the lifetime hierarchy places the Ω_c^0 baryon as having the second largest lifetime after the Ξ_c^+ baryon, $\tau_{\Xi_c^+} > \tau_{\Omega_c^0} > \tau_{\Lambda_c^+} > \tau_{\Xi_c^0}$.

4.3 Rare decays

A search for the decay $B_s^0 \rightarrow \bar{K}^{*0} \mu^+ \mu^-$ has been performed using the full Run 1 dataset and 1.6 fb^{-1} from Run 2 [23]. The decay $B_s^0 \rightarrow \bar{K}^*(892)^0 \mu^+ \mu^-$, hereafter referred to as $B_s^0 \rightarrow \bar{K}^{*0} \mu^+ \mu^-$, proceeds via a $b \rightarrow d$ flavour-changing neutral-current (FCNC) transition and the Standard Model predictions for the branching fraction of the decay are in the range $(3\text{--}4) \times 10^{-8}$. This decay is extremely interesting as it is the partner of $b \rightarrow sl^+l^-$ decays where several intriguing anomalies are observed. Searching for the decay, an excess is found over the background-only hypothesis with a significance of 3.4 standard deviations. The branching fraction of the $B_s^0 \rightarrow \bar{K}^{*0} \mu^+ \mu^-$ decay is determined to be $\mathcal{B}(B_s^0 \rightarrow \bar{K}^{*0} \mu^+ \mu^-) = [2.9 \pm 1.0 (\text{stat}) \pm 0.2 (\text{syst}) \pm 0.3 (\text{norm})] \times 10^{-8}$, where the first and second uncertainties are statistical and systematic, respectively. The third uncertainty is due to limited knowledge of external parameters used to normalise the branching fraction measurement. This measurement is consistent with existing SM predictions of the branching fraction of the decay and a SM-like value of $|V_{td}/V_{ts}|$. A detailed

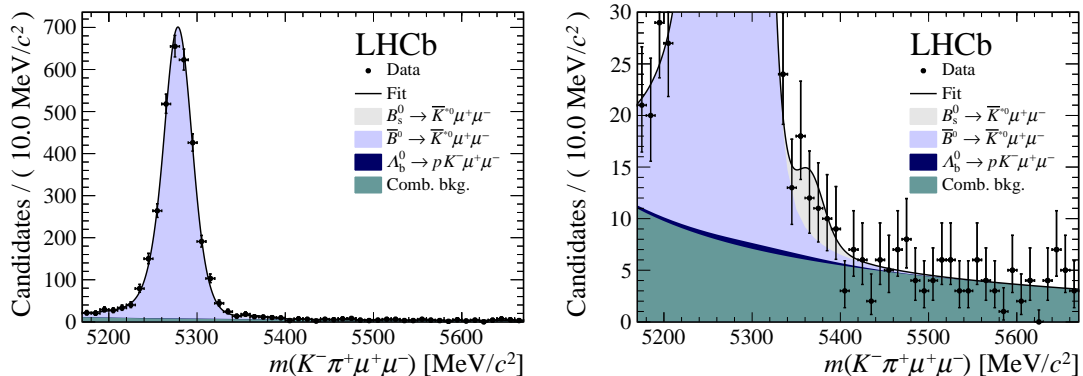


Figure 15: Distribution of reconstructed $K^-\pi^+\mu^+\mu^-$ invariant mass. The candidates are shown (left) over the full range and (right) over a restricted vertical range to emphasise the $B_s^0 \rightarrow \bar{K}^{*0}\mu^+\mu^-$ component.

analysis of the q^2 spectrum of the $B_s^0 \rightarrow \bar{K}^{*0}\mu^+\mu^-$ decay requires a larger data set. Such a data set should be available with the upgraded LHCb experiment [24].

Semileptonic decays of B mesons to excited charm states act as important backgrounds to decay channels such as $B \rightarrow D\ell\nu$ and $B \rightarrow D^*\ell\nu$ that are central for experimental tests of lepton flavor universality. However the composition of the inclusive bottom-to-charm semileptonic rate is not fully understood and one way to resolve this issue is to make measurements of relative rates between different final states. The contribution of excited states to the total semileptonic rate can be studied using B decays in which the B momentum is known. This allows one to calculate the mass of the undetected or “missing” part of the decay, and thus separate different excited D states. The decay of the narrow resonance $\bar{B}_{s2}^{*0} \rightarrow B^- K^+$ has been used by LHCb to determine the B^- momentum in partially reconstructed decays without any assumptions on the decay products of the B^- meson [25]. This technique is employed for the first time to distinguish contributions from D^0 , D^{*0} , and higher-mass charmed states (D^{**0}) in semileptonic B^- decays by using the missing-mass distribution. The measurement is performed using Run 1 data. The resulting branching fractions relative to the inclusive $B^- \rightarrow D^0 X \mu^- \bar{\nu}_\mu$ are $f_{D^0} = \mathcal{B}(B^- \rightarrow D^0 \mu^- \bar{\nu}_\mu) / \mathcal{B}(B^- \rightarrow D^0 X \mu^- \bar{\nu}_\mu) = 0.25 \pm 0.06$, $f_{D^{**0}} = \mathcal{B}(B^- \rightarrow (D^{**0} \rightarrow D^0 X) \mu^- \bar{\nu}_\mu) / \mathcal{B}(B^- \rightarrow D^0 X \mu^- \bar{\nu}_\mu) = 0.21 \pm 0.07$, with $f_{D^{*0}} = 1 - f_{D^0} - f_{D^{**0}}$ making up the remainder.

Flavour changing neutral current transitions $b \rightarrow sl^+l^-$ are investigated at LHCb in many different channels. Baryon decays are extremely interesting in this respect. In the SM, the decay $\Lambda_b^0 \rightarrow \Lambda \mu^+ \mu^-$ has a branching fraction of order 10^{-6} [26]. In extensions of the SM the branching fraction and angular distribution of the decay can be modified significantly, with the latter providing a large number of particularly sensitive observables. This decay therefore provides an important additional test of the SM predictions, which can be used to improve our understanding of the nature of the anomalies seen in the B meson decays. An analysis

of the angular distribution was reported in a recent publication [27], using Run 1 and Run 2 data corresponding to an integrated luminosity of approximately 5 fb^{-1} . Angular observables are determined using a moment analysis of the angular distribution at low hadronic recoil, corresponding to the dimuon invariant mass squared range $15 < q^2 < 20 \text{ GeV}^2/c^4$. The full basis of observables is measured for the first time and the results are found to be consistent with the SM expectations.

4.4 Searches

LHCb is pursuing a wide programme of searches for exotic states. Many exotic hadrons have been observed especially in the charmonium sector. However, no exotic hadron that is composed of more than two heavy quarks has been observed so far. Recently, several predictions for the mass and width of an exotic state, $X_{\bar{b}bb\bar{b}}$, with quark composition $b\bar{b}b\bar{b}$ have been reported. Observation of $\Upsilon(1S)\Upsilon(1S)$ production has also been reported by the CMS collaboration [28]. LHCb has studied the $\Upsilon(1S)\mu^+\mu^-$ invariant-mass distribution looking for a possible exotic meson state composed of two b quarks and two \bar{b} quarks, using Run 1 and Run 2 data corresponding to 6.3 fb^{-1} . No significant excess was found, and upper limits of order $\mathcal{O}(10 \text{ fb})$ are set on the product of the production cross-section and the branching fraction of the hypothetical $X_{\bar{b}bb\bar{b}}$ state as a function of its mass.

Searches are extended also to new processes foreseen in models beyond the SM. Decays mediated by charged-lepton flavour-violating (CLFV) processes are forbidden in the SM and their observation would be a clear sign for physics beyond the SM. The LEP experiments set stringent limits on the CLFV decay of the Z boson. In the presence of CLFV couplings, the decays to $e^\pm\mu^\mp$, $e^\pm\tau^\mp$ and $\mu^\mp\tau^\mp$ could be mediated by a Higgs boson for example in scenarios like that of a hidden gauge sector. In this context, the BaBar and Belle collaborations have performed searches for a resonance with a mass below $10 \text{ GeV}/c^2$. A search for Higgs-like bosons decaying via a lepton-flavour-violating process $H \rightarrow \mu^\pm\tau^\mp$ has been performed by LHCb in the mass range $45\text{--}195 \text{ GeV}/c^2$, using Run 1 data at $\sqrt{s} = 8 \text{ TeV}$. No signal has been found and upper bounds on the cross-section multiplied by the branching fraction were set ranging from 22 pb for $m_H = 45 \text{ GeV}/c^2$ to 4 pb for $m_H = 195 \text{ GeV}/c^2$.

4.5 Physics at fixed target

LHCb continues to produce important results obtained in fixed target mode, exploiting the gas target provided through the SMOG (System to Measure the Overlap integral with Gas) system. In a recent paper [7], LHCb reported the first measurement of prompt \bar{p} production in pHe collisions using the LHC beam impinging on a He gas target. The antiproton fraction in cosmic rays has been long recognized as a sensitive indirect probe for exotic astrophysical sources of antimatter, such as dark matter annihilation. A substantial improvement in experimental precision on the measurement of the antiproton, \bar{p} , over proton, p , flux ratio has recently been

achieved by the space-borne PAMELA and AMS-02 experiments. In particular the latter reports an excess of \bar{p} yields over current predictions for known production mechanisms. However, this excess can still be accommodated within the current uncertainties which in the 10–100 GeV \bar{p} energy range are dominated by the limited knowledge of the \bar{p} production cross-section in the relevant processes. To date, no direct measurements of \bar{p} production in pHe collisions have been made, and no data are available at a nucleon-nucleon center-of-mass energy of $\sqrt{s_{NN}} \sim 100$ GeV, relevant for the production of cosmic antiprotons above 10 GeV.

LHCb studied the prompt \bar{p} production in pHe collisions using a proton beam with an energy of 6.5 TeV impinging on a helium gas target, at a corresponding center-of-mass energy $\sqrt{s_{NN}} = 110$ GeV. The forward geometry and particle identification (PID) capabilities of the LHCb detector are exploited to reconstruct antiprotons with momentum, p , ranging from 12 to 110 GeV/ c and transverse momentum, p_T , between 0.4 and 4.0 GeV/ c . The integrated luminosity is determined from the yield of elastically scattered atomic electrons. The measurement has been performed using a sample of pHe collisions corresponding to an integrated luminosity of 0.5 nb^{-1} . The precision is limited by systematic effects and is better than a relative 10% for most kinematic bins, well below the spread among models describing \bar{p} production in nuclear collisions. The measured cross-section as a function of momentum, integrated over various p_T regions, and compared to several theoretical models is shown in Fig. 16. The energy scale, $\sqrt{s_{NN}} = 110$ GeV, and the measured range of the antiproton kinematic spectrum are crucial for improving the precision of the secondary \bar{p} cosmic ray flux prediction, and thus for interpreting the \bar{p} cosmic ray measurements from the PAMELA and AMS-02 experiments. These results represent the first direct determination of the antiproton production cross-section in pHe collision.

5 Financial issues

The status of the accounts is healthy and no cash flow problems are foreseen. The expenditure on the 2017 M&O Cat. A budget followed well our forecasts. An overspending of 6% is registered, due to the decision to anticipate the acquisition of storage components. Therefore year 2017 has followed expectation and expenditures are in line with a well balanced budget. Year 2018 is expected also to be well balanced, according to the end of August analysis and numbers. A financial plan, regarding M&O cat.A levels for the forthcoming LS2 and successive upgrade phase has been finalised, submitted and approved by the Scrutiny Group and by the RRB in Oct. 2017.

6 Collaboration matters

Three new groups joined LHCb, Laboratory of Mathematical and Subatomic Physics, Constantine, Algeria, Institute Of High Energy Physics (IHEP), Beijing,

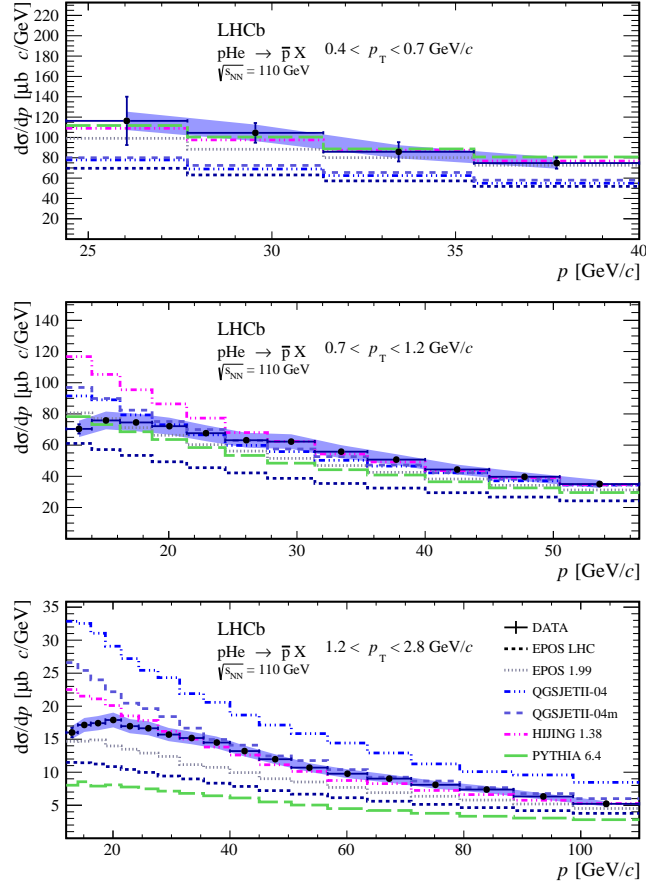


Figure 16: Antiproton production cross-section as a function of momentum, integrated over various p_T regions [7]. The data points are compared with predictions from theoretical models. The uncertainties on the data points are uncorrelated only, while the shaded area indicates the correlated uncertainty.

China, South China Normal University, Guangzhou, China. Two additional groups were upgraded from associate to full members, University of Chinese Academy of Sciences, Beijing, China and Institute of Particle Physics, Central China Normal University, Wuhan, Hubei, China. Finally, the first Technical Associate group, Jozef Stefan Institute, Ljubljana, Slovenia, joined the collaboration.

References

- [1] LHCb collaboration, R. Aaij *et al.*, *Measurement of the CKM angle γ using $B^\pm \rightarrow DK^\pm$ with $D \rightarrow K_S^0 \pi^+ \pi^-$, $K_S^0 K^+ K^-$ decays*, JHEP **08** (2018) 176, [arXiv:1806.01202](#).
- [2] LHCb collaboration, *Update of the LHCb combination of the CKM angle γ using $B \rightarrow DK$ decays*, LHCb-CONF-2018-002.
- [3] LHCb collaboration, R. Aaij *et al.*, *Measurement of CP asymmetries in two-body $B_{(s)}^0$ -meson decays to charged pions and kaons*, Phys. Rev. **D98** (2018) 032004, [arXiv:1805.06759](#).
- [4] LHCb collaboration, R. Aaij *et al.*, *Observation of the doubly charmed baryon Ξ_{cc}^{++}* , Phys. Rev. Lett. **119** (2017) 112001, [arXiv:1707.01621](#).
- [5] LHCb collaboration, R. Aaij *et al.*, *Measurement of the lifetime of the doubly charmed baryon Ξ_{cc}^{++}* , Phys. Rev. Lett. **121** (2018) 052002, [arXiv:1806.02744](#).
- [6] LHCb collaboration, R. Aaij *et al.*, *Measurement of the Ω_c^0 lifetime*, Phys. Rev. Lett. **121** (2018) 092003, [arXiv:1807.02024](#).
- [7] LHCb collaboration, R. Aaij *et al.*, *Measurement of antiproton production in pHe collisions at $\sqrt{s_{NN}} = 110$ GeV*, [arXiv:1808.06127](#), submitted to Phys. Rev. Lett.
- [8] LHCb collaboration, *Status of the LHCb upgrade*, CERN-RRB-2018-053.
- [9] C. Abellan Beteta *et al.*, *Monitoring radiation damage in the LHCb Tracker Turicensis*, [arXiv:1809.05063](#).
- [10] C. Bozzi, *LHCb Computing Resource usage in 2017*, Tech. Rep. LHCb-PUB-2018-002. CERN-LHCb-PUB-2018-002, CERN, Geneva, Mar, 2018.
- [11] C. Bozzi, *LHCb Computing Resources: 2019/2020 requests and preview of Run 3 computing model*, Tech. Rep. LHCb-PUB-2018-011. CERN-LHCb-PUB-2018-011, CERN, Geneva, Sep, 2018.
- [12] LHCb collaboration, R. Aaij *et al.*, *Determination of γ and $-2\beta_s$ from charmless two-body decays of beauty mesons*, Phys. Lett. **B739** (2015) 1, [arXiv:1408.4368](#).
- [13] LHCb collaboration, R. Aaij *et al.*, *Measurement of CP violation in $B^0 \rightarrow D^\pm \pi^\mp$ decays*, JHEP **06** (2018) 084, [arXiv:1805.03448](#).
- [14] LHCb, I. Bediaga *et al.*, *Physics case for an LHCb Upgrade II - Opportunities in flavour physics, and beyond, in the HL-LHC era*, [arXiv:1808.08865](#).

- [15] CKMfitter group, J. Charles *et al.*, *Current status of the Standard Model CKM fit and constraints on $\Delta F = 2$ new physics*, Phys. Rev. **D91** (2015) 073007, [arXiv:1501.05013](https://arxiv.org/abs/1501.05013), updated results and plots available at <http://ckmfitter.in2p3.fr/>.
- [16] UTfit collaboration, M. Bona *et al.*, *The unitarity triangle fit in the standard model and hadronic parameters from lattice QCD: A reappraisal after the measurements of Δm_s and $BR(B \rightarrow \tau\nu_\tau)$* , JHEP **10** (2006) 081, [arXiv:hep-ph/0606167](https://arxiv.org/abs/hep-ph/0606167), updated results and plots available at <http://www.utfit.org/>.
- [17] Heavy Flavor Averaging Group, Y. Amhis *et al.*, *Averages of b -hadron, c -hadron, and τ -lepton properties as of summer 2016*, Eur. Phys. J. **C77** (2017) 895, [arXiv:1612.07233](https://arxiv.org/abs/1612.07233), updated results and plots available at <https://hflav.web.cern.ch>.
- [18] LHCb collaboration, *Measurement of the CKM angle γ from a combination of $B \rightarrow DK$ analyses*, LHCb-CONF-2017-004. Retired Conference note. Please do not cite it.
- [19] LHCb collaboration, R. Aaij *et al.*, *Observation of D^0 meson decays to $\pi^+\pi^-\mu^+\mu^-$ and $K^+K^-\mu^+\mu^-$ final states*, Phys. Rev. Lett. **119** (2017) 181805, [arXiv:1707.08377](https://arxiv.org/abs/1707.08377).
- [20] LHCb collaboration, R. Aaij *et al.*, *Measurement of angular and CP asymmetries in $D^0 \rightarrow \pi^+\pi^-\mu^+\mu^-$ and $D^0 \rightarrow K^+K^-\mu^+\mu^-$ decays*, Phys. Rev. Lett. **121** (2018) 091801, [arXiv:1806.10793](https://arxiv.org/abs/1806.10793).
- [21] LHCb collaboration, R. Aaij *et al.*, *First observation of the doubly charmed baryon decay $\Xi_{cc}^{++} \rightarrow \Xi_c^+\pi^+$ decay*, [arXiv:1807.01919](https://arxiv.org/abs/1807.01919), submitted to Phys. Rev. Lett.
- [22] Particle Data Group, M. Tanabashi *et al.*, *Review of particle physics*, Phys. Rev. **D98** (2018) 030001.
- [23] LHCb collaboration, R. Aaij *et al.*, *Evidence for the decay $B_s^0 \rightarrow \bar{K}^{*0}\mu^+\mu^-$* , JHEP **07** (2018) 020, [arXiv:1804.07167](https://arxiv.org/abs/1804.07167).
- [24] LHCb collaboration, *Framework TDR for the LHCb Upgrade: Technical Design Report*, CERN-LHCC-2012-007.
- [25] LHCb collaboration, R. Aaij *et al.*, *Measurement of the relative $B^- \rightarrow D^0 X \mu^- \bar{\nu}_\mu$ branching fractions using B^- mesons from B_{s2}^{0*} decays*, [arXiv:1807.10722](https://arxiv.org/abs/1807.10722), submitted to Phys. Rev. D.
- [26] W. Detmold and S. Meinel, *$A_b^0 \rightarrow A\ell^+\ell^-$ form factors, differential branching fraction, and angular observables from lattice QCD with relativistic b quarks*, Phys. Rev. **D93** (2016) 074501, [arXiv:1602.01399](https://arxiv.org/abs/1602.01399).

- [27] LHCb collaboration, R. Aaij *et al.*, *Angular moments of the decay $\Lambda_b^0 \rightarrow \Lambda \mu^+ \mu^-$* , arXiv:1808.00264, submitted to JHEP.
- [28] CMS collaboration, V. Khachatryan *et al.*, *Observation of $\Upsilon(1S)$ pair production in proton-proton collisions at $\sqrt{s} = 8$ TeV*, JHEP **05** (2017) 013, arXiv:1610.07095.